Transport aspects in anomalous diffusion: Lévy walks

A. Blumen
Physics Institute and Bayreuther Institut für Makromolekülforschung, University of Bayreuth, D-8580 Bayreuth, West Germany

G. Zumofen
Laboratorium für Physikalische Chemie, Eidgenössische Technische Hochschule–Zentrum, CH-8092 Zürich, Switzerland

J. Klafter
School of Chemistry, Tel-Aviv University, Tel-Aviv, 69978 Israel
(Received 7 March 1989)

In this paper we present a combined analytical and numerical study of transport properties of Lévy walks. Here, within the framework of continuous-time random walks (CTRW's) with coupled memories, we focus on the probability $P_0(t)$ of being at the initial site at time t and on $S(t)$, the mean number of distinct sites visited in time t. We use the connection between $P_0(t)$ and $S(t)$, which are related via their Laplace transform, and we reanalyze our previous findings for $\langle r^2(t)\rangle$, the mean-squared displacement. Furthermore, $S(t)$ shows, as a function of the memory parameters, a very interesting, nonuniversal, nonmonotonic behavior, which we corroborate by numerical simulations in one dimension. We compare the findings with those for decoupled CTRW's on regular lattices and on fractals.

I. INTRODUCTION

Recently, much research has centered on dynamical processes in disordered media. Interestingly such processes may differ, however, from simple Brownian motion, a fact manifested through the dependence of the mean-squared displacement $\langle r^2(t)\rangle$ on time. Whereas for simple diffusion $\langle r^2(t)\rangle \sim t$, anomalous diffusion is characterized by

$$\langle r^2(t)\rangle \sim t^{\alpha} \tag{1}$$

with $\alpha \neq 1$. Examples for Eq. (1) are to be found in chaotic dynamics, which generally leads to enhanced diffusion (e.g., for turbulent motion $\alpha \simeq 3$) on the one hand,[1–9] but also in systems with geometric constraints (doped crystals, glasses, fractals), for which the diffusion is dispersive, i.e., $\alpha < 1$, on the other hand.[10–14]

Another quantity, which is of relevance in transport phenomena,[14] the mean number of distinct sites visited, shows the proportionality

$$S(t) \sim t^{\beta}, \tag{2}$$

where $\beta = 1$ for regular random walks in three-dimensional (3D) ordered systems. $\beta < 1$ is found in low dimensions,[15] restricted geometries,[12] and amorphous systems.[14]

In a review article[14] we have summarized the different models—continuous-time random walks (CTRW's), fractals, and also ultrametric spaces (UMS)—which give rise to $\alpha < 1$ and $\beta < 1$. As noted above, in turbulent motion in fluids one encounters a *superlinear* dependence of the mean-squared displacement between two particles as a function of time,[1–7] typical values of α in Eq. (1) being around $\alpha = 3$. This result is remarkable, since for correlated simple random walks or for coherent motion [where $\langle r(t)\rangle \sim t$] one attains at most $\alpha = 2$. The finding $\alpha \simeq 3$ is due to the eddy structures of fully developed turbulence, for which a complete microscopic understanding is still lacking.

An analytical approach based on asymptotic expansions has been developed by us in recent work.[8,9] There both patterns of anomalous diffusion follow from an integro-differential approach, whose basis is continuous-time random walks.[10,13,15–17] The main ingredients of this approach are spatio-temporal couplings,[18,19] which give rise to Lévy walks.[19–22] The formalism connects the dispersive region $\alpha < 1$, which obtains from temporal and geometric constraints, with the region $\alpha > 1$, typical for chaotic dynamics and turbulence.

In this paper we present a combined analytical and numerical approach for the determination of $P(\mathbf{r},t)$ and of $S(t)$ for different parameters of the coupled memories. Here, $P(\mathbf{r},t)$, the probability of being at $\mathbf{r}$ at time t, plays a central role, since its Fourier-Laplace transform $\rho(\mathbf{k},u)$ is simply related both to $S(t)$ and also to $\langle r^2(t)\rangle$, the mean-squared displacement. Of importance is the limit $u \to 0$, k small. Furthermore, the analysis makes extensive use of the coupled-memory term, which in the Fourier-Laplace space is written $\psi(\mathbf{k},u)$. For long times the limiting behavior $u \to 0$ is required. Now, in the calculation of $\langle r^2(t)\rangle$ also the limit $\mathbf{k} \to 0$ is needed, and care has to be taken to the order in which the limiting process has to be performed, since one should have $k \ll u$. On the other hand, for the calculation of $S(t)$ the full k behavior is needed and the k values with $k \gg u$ usually contribute most. We find that $S(t)$ displays a very rich behavior, since β turns out to be a nonuniversal,

nonmonotonic function of the parameters involved in the coupled-memory term.

The paper is structured as follows. In Sec. II we recall the basic features of CTRW with coupled memories. In Sec. III we evaluate $\rho(\mathbf{k},u)$ for different memory terms and apply the results to the calculation of $S(t)$ and $\langle r^2(t)\rangle$. Section IV is devoted to numerical examples. We close the paper with a comparison with other types of random walks, both on regular and on hierarchical structures. The mathematical details on the $\psi(\mathbf{k},u)$ behavior are presented in the Appendix.

II. CONTINUOUS-TIME RANDOM WALKS

An efficient way to treat the dynamics of stochastic processes consists in following the trajectories of discrete particles: For a discrete underlying space this leads to random walks.[23]

We now recall the basic ingredients of random walks in continuous time, the so-called CTRW.[15,23,24] Let $\psi(\mathbf{r},t)$ be the probability distribution of making a step of length $\mathbf{r}$ in the time interval t to $t+dt$. The total transition probability in this time interval is

$$\psi(t)=\sum_{\mathbf{r}}\psi(\mathbf{r},t)=\psi(\mathbf{k}=0,t) \tag{3}$$

(where, in the last expression we reverted to the Fourier space, $\mathbf{r}\rightarrow\mathbf{k}$). Furthermore the survival probability at the initial site is

$$\Phi(t)=1-\int_0^t\psi(\tau)d\tau\ , \tag{4}$$

so that, switching to the Laplace space ($t\rightarrow u$) one has

$$\Phi(u)=[1-\psi(u)]/u\ . \tag{5}$$

Now the probability density $\eta(\mathbf{r},t)$ of just arriving at $\mathbf{r}$ in the time interval t to $t+dt$ follows in the usual way:[15,24]

$$\eta(\mathbf{r},t)=\sum_{\mathbf{r}'}\int_0^t\eta(\mathbf{r}',\tau)\psi(\mathbf{r}-\mathbf{r}',t-\tau)d\tau+\delta(t)\delta_{\mathbf{r},0}\ . \tag{6}$$

Here we have incorporated the initial condition of starting at $t=0$ from $\mathbf{r}=\mathbf{0}$. Equation (6) leads to an integral equation for the probability $P(\mathbf{r},t)$ that the particle is at $\mathbf{r}$ at time t, by observing that

$$P(\mathbf{r},t)=\int_0^t\eta(\mathbf{r}',t-\tau')\Phi(\tau')d\tau'\ . \tag{7}$$

With Eq. (7) and a change in the order of the integrations, Eq. (6) takes the form

$$P(\mathbf{r},t)=\sum_{\mathbf{r}'}\int_0^t P(\mathbf{r}',\tau)\psi(\mathbf{r}-\mathbf{r}',t-\tau)d\tau+\Phi(t)\delta_{\mathbf{r},0}\ . \tag{8}$$

From the last expression one has, in Fourier-Laplace space,

$$\rho(\mathbf{k},u)=\rho(\mathbf{k},u)\psi(\mathbf{k},u)+\Phi(u) \tag{9}$$

with the solution

$$\rho(\mathbf{k},u)=\frac{1-\psi(u)}{u}\frac{1}{1-\psi(\mathbf{k},u)}\ . \tag{10}$$

We may thus view Eqs. (8) and (10) in their general form as the natural extension of diffusive processes to random media, the functional $\psi(\mathbf{r},t)$ form resulting from different types of disorder. For particular cases, such as ordered arrays,[15] decoupled memories, i.e.,

$$\psi(\mathbf{r},t)=\lambda(\mathbf{r})\psi(t) \tag{11}$$

apply, for which the analysis is much simplified. In general, however, the ensemble-average transport through substitutionally disordered media obeys the CTRW Eq. (8), with a probability distribution $\psi(\mathbf{r},t)$ in which $\mathbf{r}$ and t are *coupled*.[18] Attention should also be drawn to the fact that a careful use of the projection operator technique has shown that there can also appear inhomogeneous terms which must be included when the initial conditions are not uniform.[25]

Basic quantities in our further analysis are the mean waiting time per step

$$\tau_1=\int dt\,t\int\psi(\mathbf{r},t)d\mathbf{r} \tag{12}$$

and the mean-squared displacement per step

$$\sigma^2=\int dt\int r^2\psi(\mathbf{r},t)d\mathbf{r}\ . \tag{13}$$

In Ref. 8 it was shown that for decoupled memories the mean-squared displacement is either divergent or increases sublinearly or at most linearly in time. In order to obtain finite $\langle r^2(t)\rangle$ with a superlinear temporal behavior *coupled* $\psi(\mathbf{r},t)$ forms have to be applied.[7–9,18,20] A suitable function is

$$\psi(\mathbf{r},t)=Ar^{-\mu}\delta(r-t^{\nu}) \tag{14}$$

where, through the δ function, r and t are coupled. These processes are also called Lévy walks.[19–22] Equation (14) allows steps of *arbitrary* length (as for Lévy flights[19]), but long steps are penalized by requiring longer time to be

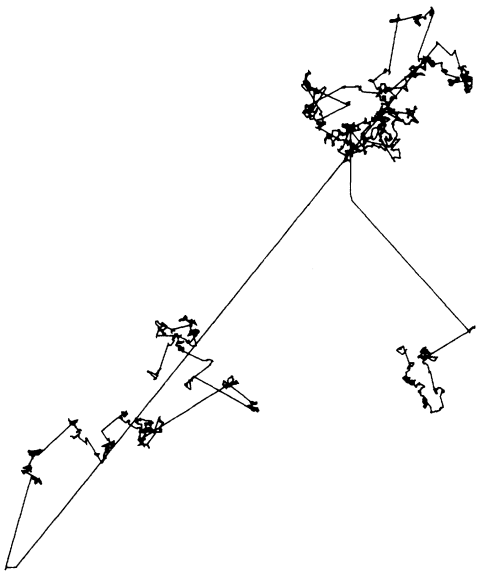

FIG. 1. Realization of a Lévy walk, obtained from the distribution probability Eq. (14), where $\mu=3.5$ and $\nu=1$. The situation depicted evolved after 3000 steps.

performed. Or, stated differently, in a given time window only a finite shell of points may be reached: hierarchically, nearer points are no more and farther points not yet accessible.

To visualize a realization of such a Lévy walk we present in Fig. 1 the situation for a two-dimensional geometry where we chose $\mu=3.5$ and $\nu=1$. One should remark the self-similar aspect of the picture: a series of small steps is followed by larger ones, which are, after a while, followed by larger ones still; furthermore, no particular length scale dominates. Figure 1 may be compared to the very similar Figs. 296 and 297 of Ref. 26.

To close this section we again stress that the CTRW model results in enhanced diffusion when a spatio-temporal coupled memory is used.[7–9,18–20] We will document this statement in the next section, where we will apply this memory form to compute the mean-squared displacement $\langle r^2(t)\rangle$ and the mean number of distinct sites visited, $S(t)$.

III. APPLICATION OF THE COUPLED MEMORIES TO $\langle r^2(t)\rangle$ AND $S(t)$

We begin this section by deriving the space-averaged waiting time distribution

$$\begin{aligned}\psi(u)&=\int_0^\infty dt\int_\theta^\infty d\mathbf{r}\,\psi(\mathbf{r},t)e^{-ut}\\&=A\int_0^\infty\int_{\theta_1}^\infty dr\,r^{d-\mu-1}\delta(r-t^\nu)e^{-ut}dt\\&=A\int_{\theta_2}^\infty t^{\nu(d-\mu-1)}e^{-ut}dt=A\int_{\theta_2}^\infty t^{-\nu\mu^*}e^{-ut}dt\end{aligned}\tag{15}$$

where we set $\mu^*=\mu-d+1$ and indicated the lower-bound cutoffs by θ_i, using the relation $\theta_2=\theta_1^{1/\nu}$. The quantity θ may be viewed as describing the distance of nearest approach between active centers; for molecules in condensed matter this would correspond to the average nearest-neighbor intermolecular spacing. From the normalization condition $\psi(u=0)=1$ one finds a lower bound for the exponent: $\nu\mu^*>1$. Moreover, a finite τ_1 obtains for $\nu\mu^*>2$. Hence, for the asymptotic expansion of $\psi(u)$ it follows that

$$\psi(u)=\begin{cases}1-Cu^{\nu\mu^*-1}, & 1<\nu\mu^*\le 2\\ 1-\tau_1 u, & \nu\mu^*>2\ .\end{cases}\tag{16}$$

The analysis of $\psi(\mathbf{k},u)$ is more involved and requires attention to the small $(\mathbf{k},u)$ expansion, depending on whether $k\ll u$ or $k\gg u$. The former case is relevant for the mean-squared displacement, as is evident from the relation

$$\langle r^2(t)\rangle=\int\mathbf{r}^2P(\mathbf{r},t)d\mathbf{r}=-\frac{\partial^2}{\partial\mathbf{k}^2}\rho(\mathbf{k},t)\Big|_{\mathbf{k}=0}\tag{17}$$

where the right-hand side may be found by an expansion in $\mathbf{k}$. As is obvious one has

$$\begin{aligned}\psi(\mathbf{k},u)-\psi(u)&=\int_0^\infty dt\int_\theta^\infty d\mathbf{r}(e^{i\mathbf{k}\cdot\mathbf{r}}-1)\psi(\mathbf{r},t)e^{-ut}\\&=A\int_0^\infty dt\,e^{-ut}\int_{\theta_1}^\infty dr\,r^{-\mu^*}\int_{-1}^1 d(\cos\varphi)(e^{ikr\cos\varphi}-1)\delta(r-t^\nu)\\&=A\int_{\theta_2}^\infty dt\,e^{-ut}t^{-\nu\mu^*}\int_{-1}^1 dx(e^{ikt^\nu x}-1)\ .\end{aligned}\tag{18}$$

For $kt^\nu\ll ut$ the term in brackets changes little during the decay of $\exp(-ut)$ and may be expanded in powers of k. Thus for $k\ll u$ this results in

$$\begin{aligned}\psi(\mathbf{k},u)-\psi(u)&\sim-k^2\int_{\theta_2}^\infty t^{-\nu(\mu^*-2)}e^{-ut}dt\\&\equiv-k^2I(u)\ .\end{aligned}\tag{19}$$

For $\nu(\mu^*-2)>1$, the integral $I(u)$ is finite for all u, even for $u=0$. For $\nu(\mu^*-2)<1$ we find that $I(u)$ diverges for $u=0$, only for $u>0$ the integral is finite. Therefore

$$\psi(\mathbf{k},u)-\psi(u)\sim\begin{cases}-C_1k^2, & \nu\mu^*>1+2\nu\\ -C_1k^2u^{\nu(\mu^*-2)-1}, & \nu\mu^*<1+2\nu\ .\end{cases}\tag{20}$$

From Eqs. (16) and (20) it is now obvious that four different cases may arise. We begin with the cases in which τ_1 is finite, $\nu\mu^*>2$. For $\nu\mu^*>1+2\nu$ one obtains

$$\psi(\mathbf{k},u)\sim1-\tau_1u-C_1k^2\ .\tag{21}$$

Using now Eq. (10) gives

$$\rho(\mathbf{k},u)\sim\frac{\tau_1}{\tau_1u+C_1k^2}\tag{22}$$

from which, considering Eq. (17), we recover Brownian behavior, and thus $\langle r^2(t)\rangle\sim t$. For $\nu\mu^*<1+2\nu$ one finds

$$\psi(\mathbf{k},u)\sim1-\tau_1u-C_1k^2u^{\nu(\mu^*-2)-1}\ .\tag{23}$$

We note here the space-time correlation, namely, that the first k^2 term involves u. From Eqs. (10) and (23) it follows that

$$\rho(\mathbf{k},u)\sim\frac{\tau_1u^{\nu(2-\mu^*)+1}}{\tau_1u^{\nu(2-\mu^*)+2}+C_1k^2}\ .\tag{24}$$

As is amply discussed in Ref. 8, to a small k, $k\ll u$ behavior of the form

$$\rho(\mathbf{k},u)\sim\frac{1}{u}-C\frac{k^2}{u^{\alpha+1}}\tag{25}$$

corresponds an anomalous behavior for $\langle r^2(t)\rangle$, where for large t

$$\langle r^2(t)\rangle \sim t^{\alpha} \tag{26}$$

[Eq. (13) of Ref. 8]. Thus, from Eq. (24), either by differentiating twice with respect to k, as in Eq. (17), or by use of Eqs. (25) and (26) the mean-squared displacement is

$$\langle r^2(t)\rangle \sim t^{\nu(2-\mu^*)+2} . \tag{27}$$

Turning now to the cases of infinite τ_1, $1<\nu\mu^*\leq 2$, we obtain for $\nu\mu^*\geq 1+2\nu$

$$\psi(\mathbf{k},u)\sim 1-Cu^{\nu\mu^*-1}-C_1k^2 , \tag{28}$$

hence

$$\rho(\mathbf{k},u)\sim \frac{Cu^{\nu\mu^*-2}}{Cu^{\nu\mu^*-1}+C_1k^2} \tag{29}$$

and we have $\langle r^2(t)\rangle \sim t^{\nu\mu^*-1}$, i.e., dispersive transport.[10,13]

Finally, for $\nu\mu^*<1+2\nu$ it follows that

$$\psi(\mathbf{k},u)\sim 1-Cu^{\nu\mu^*-1}-C_1k^2u^{\nu(\mu^*-2)-1} \tag{30}$$

and thus

$$\rho(\mathbf{k},u)\sim \frac{Cu^{\nu\mu^*-2}}{Cu^{\nu\mu^*-1}+C_1k^2u^{\nu(\mu^*-2)-1}} . \tag{31}$$

Hence, differentiating twice with respect to k it follows that $\langle r^2(t)\rangle \sim t^{2\nu}$. This is again our expression for anomalous transport: for $\nu<\frac{1}{2}$ the transport is dispersive while for $\nu>\frac{1}{2}$ it is enhanced.

Summarizing the results for the mean-squared displacement we have for long times

$$\nu\mu^*<1+2\nu,\quad \langle r^2(t)\rangle \sim t^{2-\nu\mu^*+2\nu} , \tag{32a}$$

$$\nu\mu^*>1+2\nu,\quad \langle r^2(t)\rangle \sim t \tag{32b}$$

for $\nu\mu^*>2$ and

$$\nu\mu^*<1+2\nu,\quad \langle r^2(t)\rangle \sim t^{2\nu} , \tag{32c}$$

$$\nu\mu^*>1+2\nu,\quad \langle r^2(t)\rangle \sim t^{\nu\mu^*-1} , \tag{32d}$$

for $1<\nu\mu^*<2$. These expressions can be interpreted as follows. Keeping ν fixed while varying μ^* we observe that the exponent α reaches a plateau for small μ^*, Eq. (32c), and for large μ^*, Eq. (32b). For small μ^* we have anomalous diffusion which is either dispersive for $\nu<\frac{1}{2}$ or enhanced for $\nu>\frac{1}{2}$; for large μ^* the behavior is always Brownian. In the intermediate μ^* region, the exponent α varies linearly between the limiting cases: for $\nu<\frac{1}{2}$ $\langle r^2(t)\rangle$ is given by Eq. (32d) and for $\nu>\frac{1}{2}$ by Eq. (32a), respectively.

As pointed out above, the analysis of $\rho(\mathbf{k},u)$ is complicated for coupled $\psi(\mathbf{r},t)$, a fact which renders delicate the derivation of $S(t)$, the mean number of distinct sites visited in time t. Assuming translational symmetry for the underlying lattice there is a simple relation between $S(u)$ and $P_0(u)$. In the Laplace space one has for $P_0(t)=P(\mathbf{r}=0,t)$[15,24]

$$S(u)=[u^2P_0(u)]^{-1} \tag{33}$$

where we have set $P_0(u)=\mathcal{L}[P_0(t)]$, i.e., $P_0(u)\equiv P(\mathbf{r}=0,u)$. The calculation of $P_0(u)$ requires the Fourier back transformation of Eq. (10) at $\mathbf{r}=0$:

$$P_0(u)=\frac{1-\psi(u)}{\pi^d u}\int_0^{\pi}\frac{d\mathbf{k}}{1-\psi(\mathbf{k},u)} . \tag{34}$$

Our interest centers on long times, i.e., low u values, $u\ll 1$. Now one should remark the very important fact that the evaluation of Eq. (34) requires the knowledge of $\psi(\mathbf{k},u)$ values for k values of the order of unity. In fact these values are in many cases dominant.

Thus we are in the regime $k\gg u$. For a relatively convenient discussion in the rest of this section we restrict the treatment to one dimension; a generalization to higher dimensions will be presented elsewhere.

We continue by taking the Laplace-Fourier transform of the stepping probability, Eq. (14), which results in

$$\psi(k,u)=A\sum_r{}' \int_0^{\infty} dt\, e^{-ikr-ut}\delta(r-t^{\nu})r^{-\mu} , \tag{35}$$

where the sum runs over all integers except $r=0$. This yields

$$\psi(k,u)=2A\sum_{r>0}\cos(kr)e^{-ur^{1/\nu}}r^{-\mu-1+1/\nu} . \tag{36}$$

We obtain A from the normalization condition $\psi(0,0)=1$; thus $A=1/[2\zeta(\mu+1-1/\nu)]$ where ζ is the Riemann-ζ function.

As stated before, the analysis of $\psi(k,u)$ is delicate. We only outline the procedure here, and will refer to the Appendix for the details. The main factor is that one can, to a very good approximation, express the term $1-\psi(k,u)$ needed in the integration of Eq. (34) as

$$1-\psi(k,u)=C_1u^{\gamma}+C_2k^{\epsilon} . \tag{37}$$

As we will show in the following, this expression is also sufficient for the calculation of $P_0(u)$ and, using Eq. (33), also for the evaluation of $S(u)$ and $S(t)$.

As a first step towards establishing Eq. (37) let us consider the special cases $k=0$ and $u=0$ in Eq. (36). For $k=0$ it follows that

$$1-\psi(0,u)=2A\sum_{r>0}\frac{1-e^{-ur^{1/\nu}}}{r^{\mu+1-1/\nu}} . \tag{38}$$

The sum in Eq. (38) converges for $\mu-1/\nu>0$, i.e., $\mu\nu>1$, as stated before. If also $\mu-2/\nu>0$, i.e., $\mu\nu>2$, holds, then the leading term in Eq. (38) is proportional to u. For $1<\mu\nu<2$ we may approximate the sum by an integral over r. A change of variables, $x=ur^{1/\nu}$ shows that the leading term is now proportional to $u^{\mu\nu-1}$; in agreement with Eq. (16). The details are presented in the Appendix, and we find the following general form:

$$1-\psi(0,u)\sim C_1u^{\gamma} , \tag{39}$$

where

$$\gamma=\min(\mu\nu-1,1) \tag{40}$$

and

$$C_1\simeq\begin{cases}-2A\nu\Gamma(1-\mu\nu), & 1<\mu\nu<2\\ 2A\zeta(\mu+1-2/\nu), & \mu\nu>2\ .\end{cases} \tag{41}$$

For $u=0$ we similarly find

$$1-\psi(k,0)=2A\sum_{r>0}\frac{1-\cos(kr)}{r^{\mu+1-1/\nu}}\ . \tag{42}$$

The sum in Eq. (42) again converges for $\mu\nu>1$. If also $\mu-1/\nu-2>0$, i.e., $\mu\nu>2\nu+1$ holds, then the leading term in Eq. (42) is proportional to k^2. For $1<\mu\nu<2\nu+1$ we can again approximate the sum by an integral over r. The change of variables $x=kr$ shows that the leading term is now going as $k^{(\mu\nu-1)/\nu}$. We present the details in the Appendix. Here the general form is

$$1-\psi(k,0)\sim C_2k^{\epsilon}\ , \tag{43}$$

where

$$\epsilon=\min((\mu\nu-1)/\nu,2)\ , \tag{44}$$

$$C_2=\begin{cases}\dfrac{A\pi\,\mathrm{cosec}[(\mu-1/\nu)\pi/2]}{\Gamma(\mu+1-1/\nu)}, & \mu-1/\nu<2\\ A\zeta(\mu-1-1/\nu), & \mu-1/\nu>2\ .\end{cases} \tag{45}$$

We remark now that the additive combination of Eqs. (39) and (43) leads to the claimed expression, Eq. (37). We have carefully checked Eq. (37), by numerical evaluation of the sum in Eq. (36) for whole series of parameter values. Expression (37) holds very well, as we demonstrate in the Appendix. The only place where one has to be careful is the region $k\ll u$; as discussed before, there the functional dependence is given by Eqs. (21), (23), (28), and (30). *Numerically,* however, these equations are very similar to Eq. (37) since for $k\ll u$ the leading, u-dependent term *always* dominates.

Furthermore, logarithmic corrections arise at the crossovers between the characteristic functional dependencies in Eqs. (41) and (45). Not to burden the description any further, we disregard these corrections here.

Inserting now Eqs. (37) and (39) into Eq. (34) one has

$$P_0(u)=\frac{C_1u^{\gamma-1}}{\pi}\int_0^{\pi}\frac{dk}{C_1u^{\gamma}+C_2k^{\epsilon}}\ . \tag{46}$$

In the same vein as before, for $\epsilon<1$ the integral converges even for $u=0$. The leading term is thus proportional to $u^{\gamma-1}$. For $\epsilon>1$ the integral diverges for $u=0$, and the main contribution to the integral stems from the small k region. We can then safely extend the integration in Eq. (46) to infinity. The change of variable $x=k/u^{\gamma/\epsilon}$ shows that the leading term is now proportional to $u^{-1+\gamma/\epsilon}$. We find, therefore,

$$P_0(u)\sim\begin{cases}C_3u^{\gamma-1}, & \epsilon<1\\ C_3u^{\gamma/\epsilon-1}, & 1<\epsilon<2\end{cases} \tag{47}$$

$$C_3\simeq\begin{cases}\dfrac{C_1}{\pi^{\epsilon}(1-\epsilon)C_2}, & \epsilon<1\\ \dfrac{C_1^{1/\epsilon}}{\sin(\pi/\epsilon)\epsilon C_2^{1/\epsilon}}, & 1<\epsilon<2\ .\end{cases} \tag{48}$$

Using Eq. (47) we now calculate $S(t)$ by taking the Laplace inverted form of Eq. (33), which then gives

$$S(t)\sim\begin{cases}C_4t^{\gamma}, & \epsilon<1\\ C_4t^{\gamma/\epsilon}, & 1<\epsilon<2\end{cases} \tag{49}$$

and the prefactor C_4 is

$$C_4=\begin{cases}\dfrac{\pi^{\epsilon}(1-\epsilon)C_2}{\Gamma(1+\gamma)C_1}, & \epsilon<1\\ \dfrac{\epsilon\sin(\pi/\epsilon)C_2^{1/\epsilon}}{\Gamma(1+\gamma/\epsilon)C_1^{1/\epsilon}}, & 1<\epsilon<2\ .\end{cases} \tag{50}$$

Summarizing the results for different domains, see Eqs. (45), (48), and (49), one finds that $S(t)$ shows a rich pattern, namely, (i) for $\nu<\frac{1}{2}$ and

$$\begin{aligned}&1<\mu\nu<1+\nu,\quad S(t)\sim t^{\mu\nu-1}\ ,\\ &1+\nu<\mu\nu<1+2\nu,\quad S(t)\sim t^{\nu}\ ,\\ &1+2\nu<\mu\nu<2,\quad S(t)\sim t^{(\mu\nu-1)/2}\ ,\\ &2<\mu\nu,\quad S(t)\sim t^{1/2}\ ,\end{aligned} \tag{51a}$$

(ii) for $\frac{1}{2}\le\nu<1$ and

$$\begin{aligned}&1<\mu\nu<1+\nu,\quad S(t)\sim t^{\mu\nu-1}\ ,\\ &1+\nu<\mu\nu<2,\quad S(t)\sim t^{\nu}\ ,\\ &2<\mu\nu<1+2\nu,\quad S(t)\sim t^{\nu/(\mu\nu-1)}\ ,\\ &1+2\nu<\mu\nu,\quad S(t)\sim t^{1/2}\ ,\end{aligned} \tag{51b}$$

and (iii) for $1\le\nu$ and

$$\begin{aligned}&1<\mu\nu<2,\quad S(t)\sim t^{\mu\nu-1}\ ,\\ &2<\mu\nu<1+\nu,\quad S(t)\sim t\ ,\\ &1+\nu<\mu\nu<1+2\nu,\quad S(t)\sim t^{\nu/(\mu\nu-1)}\ ,\\ &1+2\nu<\mu\nu,\quad S(t)\sim t^{1/2}\ .\end{aligned} \tag{51c}$$

To demonstrate the typical dependence of the exponent of $S(t)$, Eq. (2), on μ and ν we have plotted in Fig. 2 the exponent β as a function of μ for various values of ν.

We interpret our results [Eqs. (51)] for $S(t)$ along the lines used for describing $\langle r^2(t)\rangle$, Eqs. (32). Keeping ν fixed and varying μ we observe that β reaches the value $\frac{1}{2}$ for large μ irrespective of ν. This corresponds to the ordinary 1D random walk and results in Brownian motion. For small and decreasing μ the exponent β drops linearly to zero. This is because for small μ values, $S(t)$ is bounded from above by the mean number of steps per time unit. It turns out that the exponent of this quantity also drops to zero for low μ values. The intermediate regime is

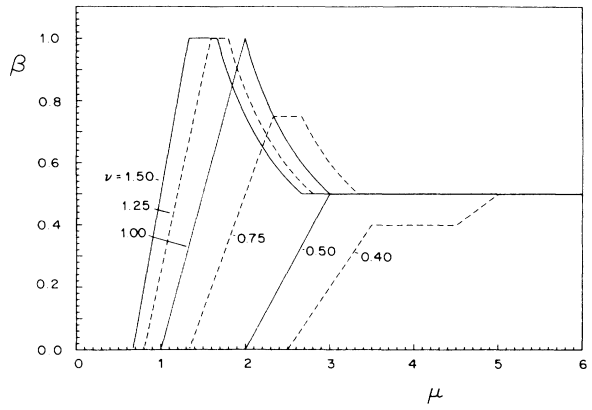

FIG. 2. Exponent β for the asymptotic behavior of $S(t)$ as a function of μ. The ν values chosen are as indicated.

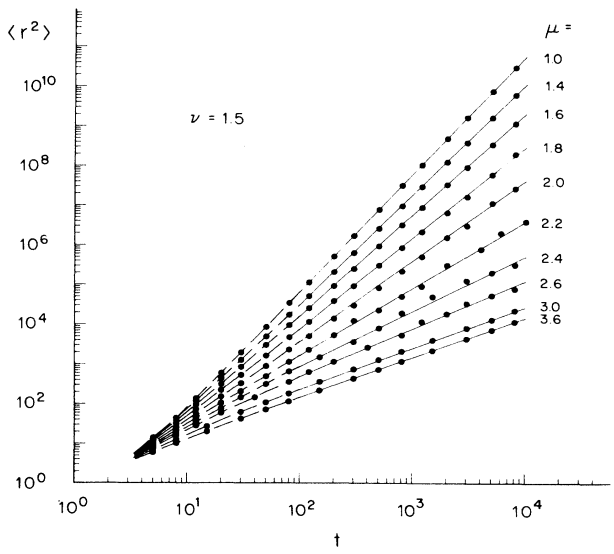

FIG. 3. The mean-squared displacement $\langle r^2(t)\rangle$ is indicated as a function of time on log-log scales. Here $\nu=\frac{3}{2}$ in Eq. (14) and μ is given parametrically. The dots are the result of simulation calculations, the solid lines denote the least-squares linear fit, and the dashed lines are guides to the eye.

governed by the enhanced or the dispersive character of the motion. For enhanced diffusion ($\nu>\frac{1}{2}$) there is a plateau with $\beta=\min(\nu,1)$ while for dispersive motion ($\nu<\frac{1}{2}$) there is a plateau with $\beta=\nu$. For the particular case $\nu=1$ the plateau shrinks to a point with $\beta=1$ at $\mu=2$. Interestingly, for $\nu>\frac{1}{2}$ there is a nonlinear transition, $\beta=\nu/(\mu\nu-1)$, between the intermediate plateau and the limiting $\beta=\frac{1}{2}$ for large μ values in accordance to a similar pattern of behavior found by Gillis and Weiss.[27]

To summarize this section, we have derived here, using coupled memories, the long-time asymptotic expressions for $\langle r^2(t)\rangle$ and $S(t)$. We have found a rich behavior which will be corroborated in the next section by simulation calculations.

IV. NUMERICAL SIMULATIONS

In order to clearly visualize the Lévy process for coupled memories and in order to be able to monitor the full time dependence of the relevant quantities (and not only their asymptotic behavior) we found it expedient to perform numerical simulations. Here we show some results for $\langle r^2(t)\rangle$ and for $S(t)$.

The procedure of the simulation is as follows. For each step one has to determine from Eq. (34) the distance and the time needed to reach the next location.[9,28] The spatial distribution of location distances follows by integrating over all times:

$$\psi(\mathbf{r})=\int_0^\infty dt\,\psi(\mathbf{r},t)=Cr^{-\xi}\,, \tag{52}$$

where $\xi=\mu+1-\nu^{-1}$. We can now choose a walking distance $\mathbf{r}$ according to the distribution (52); the time needed to travel this distance is given, considering Eq. (14), by $t=|\mathbf{r}|^{1/\nu}$. This procedure has also been used to generate the track depicted in Fig. 1. Note that for $\nu=1$ the situation is somewhat similar to random walks in which the walker steps preferentially in the same direction, the so-called persistent (or correlated) random walks.[23,24,29,30]

To analyze the mean-squared displacement in the superlinear regime we display in Fig. 3 $\langle r^2(t)\rangle$ as a function of time. We have varied μ^* between 1 and 3.6 and covered some 4 orders of magnitude in time. The whole analysis of $\langle r^2(t)\rangle$ in Sec. III centered only on $\mu^*=\mu-d+1$. We see that for $\langle r^2(t)\rangle$ the role of the dimension consists in a change from μ to μ^*, otherwise leaving everything else unchanged. We have thus for Fig. 3 simplified the simulation by taking $d=1$. For each numerical result (dot) displayed in Fig. 3, some 10^4 realizations were used in its averaging. Note the log-log scales; in these scales Eq. (1) corresponds to a straight line of slope α.

We observe that the numerical results do not lie, as a rule, on straight lines; deviations are evident, especially at early times. We have indicated these deviations as dashed curves and used only the numerical results in the late time domain for a least-squares (linear regression) fit.

We summarize in Fig. 4 the slopes α obtained from the least-squares fit for $\nu=1$ and 1.5. The overall behavior supports very nicely the analytical expressions, Eqs. (32) of Sec. III. Indeed, the transition regimes $2<\mu^*<3$ for $\nu=1$ and $\frac{4}{3}<\mu^*<\frac{8}{3}$ for $\nu=1.5$ are clearly visible. Furthermore, in both cases the regimes of enhanced diffusion ($\alpha=3$ or $\alpha=2$, respectively) and of regular diffusion ($\alpha=1$) are reached within the time of the numerical experiment.

In Fig. 4 we have also indicated through solid lines the theoretically predicted behavior. Whereas the general agreement is good, we also remark that the numerical crossover behavior is considerably *smoother* than theoretically expected: we attribute this to the very long times which are required to reach the asymptotic regime of

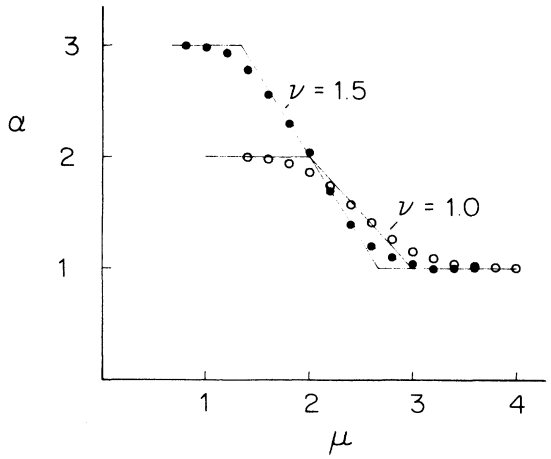

FIG. 4. Summary of the numerically determined asymptotic behavior from Figs. 3 and 4. The slopes α are presented as a function of μ; we use dots for $\nu=\frac{3}{2}$ and circles for $\nu=1$. The solid lines give the analytically expected behavior, Eqs. (32).

$\langle r^2(t)\rangle$ for marginal values of μ^* ($\mu^*=2$ and $\mu^*=3$, or $\mu^*=\frac{4}{3}$ and $\mu^*=\frac{8}{3}$, respectively).

The results of a numerical analysis of $S(t)$ are shown in Fig. 5. Displayed is $S(t)$ as a function of t on a log-log scale for $d=1$ and $\nu=1$. We have varied μ between 1.2 and 6. As for $\langle r^2(t)\rangle$ the numerical results of $S(t)$ tend, for longer times, to straight lines. However, there are, depending on the μ values, marked differences. Whereas for $\mu\geq 3$ a straight line behavior is reached within approximately 10 time steps for $\mu<3$ it takes considerably longer.

The computed results clearly show that the slopes at $t=10^4$ reach a maximum for $\mu=2$. This finding is in agreement with the theoretical predictions shown in Fig. 2 and summarized in Eq. (51). We have also performed a linear least-squares fit for time intervals $10^3<t<10^4$. The fitted slopes follow as a rule reasonably the theoretically expected μ dependence; especially remarkable is that for μ around 1 the behavior goes clearly as $\beta=\mu-1$.

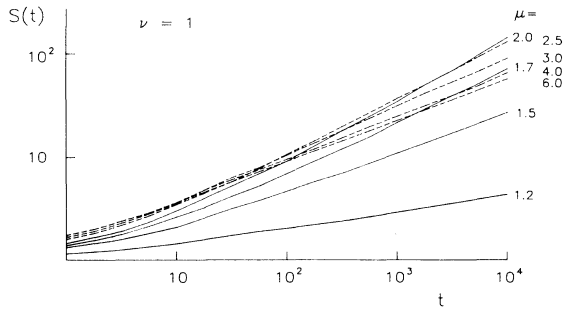

FIG. 5. The mean number of distinct sites visited, $S(t)$, is plotted as a function of time on log-log scales. Here $\nu=1$ and μ is given parametrically [for clarity the $S(t)$ curves for μ values larger than two are dashed].

Notoriously difficult for numerical simulations are transition regimes, and in this respect our system makes no exception. In the domain $2<\mu<3$ the approach to straight lines is very sluggish and the slopes computed by the regression analysis lie somewhat below the theoretically expected values; evidently for a closer agreement one would have to go to much longer times.

To close this discussion on the $S(t)$ simulations we reiterate our major finding, namely, that the dependence of the parameter β on μ is here nonmonotonic, showing a marked maximum for $\mu=2$, in excellent agreement with the theoretical expectations from Fig. 2.

V. CONCLUSIONS

In this work we have shown that CTRW's allow the straightforward extension of Brownian motion to anomalous transport, both in the dispersive and in the enhanced cases. Whereas in the CTRW framework the dispersive transport may also be obtained from decoupled kernels,[10] the enhanced diffusion can only be achieved by using kernels which couple hierarchically time and space, e.g., Eq. (14). The major advantage of using random walks preferentially to diffusion-type equations is that random walks offer a dynamical picture of the motion, which allows one to follow the course of chemical reactions in complex situations, as we have already demonstrated for dispersive motion.[31]

The particular kernel used, Eq. (14), leads to a very rich pattern in the transport phenomena. For the mean-squared displacement the enhanced diffusion of chaotic dynamics appears as a special case: the transition shows an intermediate zone between the Brownian motion and the fully developed enhanced diffusion. Interestingly, an intermediate zone is also found for dispersive transport, where the transition between Brownian behavior and largest possible dispersion is gradual.

The situation is more complex for $S(t)$, the mean number of distinct sites visited, as becomes clear from Fig. 2. Since only the turning points of the random walk are considered as sites visited, $S(t)$ may not grow faster than linear in time. The effect of enhanced diffusion is therefore only visible in low dimensions for which a sublinear behavior is expected for ordinary walks. Moreover, for small μ the exponent of $S(t)$ tends to zero, while that of $\langle r^2(t)\rangle$ reaches a plateau. These behaviors would change considerably if not only the turning points but the whole trail of the random walk track were accounted for.

Whether $S(t)$ in its present form or in a form which includes the whole trail is the relevant quantity for the description of reactions and relaxations in turbulent flows must be further investigated. However, even the $S(t)$ analysis performed here displays the richness of behavior which can be found when coupled-memory terms are investigated.

As a note, we remark that nowadays the comparison to experimental findings should be much enhanced, since careful measurements should become available. We feel that the method of choice is to use fluorescent probes,[28] which are excited by a laser, so that one attains a high spatial resolution and one does not, through the marking,

interfere with the flow process. A series of pictures of jet flows was indeed made visible through luminescence by Dimotakis *et al.*[32] Note that up to now the standard means of marking the velocity regions were by injection of color plumes or by smoke (aerosols, oil fog). These means are not very satisfactory, since one has to put the markers exactly where the vorticity is generated, which taken strictly is impossible;[33] hence on a small scale the interface is marked only roughly. For more precision one has to revert to tracking the molecules of the turbulent flow by themselves and luminescence measurements are an obvious candidate for such tracking.

Summarizing, the Lévy-walk-CTRW approach provides a unified theoretical scheme for both types of anomalous transport: dispersive motion in disordered materials and enhanced diffusion in turbulent motion. It is conjectured that spatial and temporal resolved observations of excited particles in turbulent flows could provide useful information to further our knowledge of such complex dynamical systems.

ACKNOWLEDGMENTS

A grant of computer time from the Rechenzentrum der ETH-Zürich and the support of the Deutsche Forschungsgemeinschaft (SFB 213) and of the Fonds der Chemischen Industrie (grant of an IRIS workstation) are gratefully acknowledged. We thank O. Vogt for technical assistance. One of us (J.K.) acknowledges the support of the Fund for Basic Research administered by the Israel Academy of Sciences and Humanities.

APPENDIX

In this appendix we derive some of the formulas outlined in the main text. We start with an analysis of $1-\psi(k,u)$ relevant for the integration in Eq. (34) of the main text. We begin with the two limiting cases $k=0$ and $u=0$. For $k=0$ one has Eq. (38):

$$f(u)=1-\psi(0,u)=2A\sum_{r>0}\frac{1-e^{-ur^{1/\nu}}}{r^{\mu+1-1/\nu}}\ . \tag{A1}$$

Evidently, the sum in (A1) converges for $\mu+1-1/\nu>1$, i.e., $\mu\nu>1$. For $\mu+1-2/\nu>1$, i.e., $\mu\nu>2$ we may even expand the exponent to first order in u, and we expect $1-\psi(0,u)\sim C_1u$, as we subsequently show. Consider, however, first the case $1<\mu\nu<2$. We approximate the sum by an integral, which leads to

$$f(u)\simeq 2A\int_\theta^\infty dr\frac{1-e^{-ur^{1/\nu}}}{r^{\mu+1-1/\nu}}\ , \tag{A2}$$

where $\theta\simeq 1$. Extending the integration from θ to 0 introduces only a term of the order u, which will turn out to be less than the leading contribution. We thus set $\theta=0$ in (A2) and make the variable transformation $x=ur^{1/\nu}$. Thus

$$\begin{aligned}f(u)&\simeq -2Au^{\mu\nu-1}\nu\int_0^\infty dx\,x^{-\mu\nu}(e^{-x}-1)\\&=-2Au^{\nu\mu-1}\nu\Gamma(1-\mu\nu)\ ,\end{aligned} \tag{A3}$$

where in the last line we made use of the Cauchy-Saalschütz expression for negative arguments of the Γ function,[34] remembering that $-2<-\mu\nu<-1$. Equation (A3) can also be obtained directly by integrating once by parts.

For $\mu\nu>2$ we expand the denominator of Eq. (A1) to order u and have

$$f(u)\simeq 2Au\sum_{r>0}r^{-\mu-1+2/\nu}=2A\zeta(\mu+1-2/\nu)u\ , \tag{A4}$$

where we introduced the Riemann-ζ function, Eq. (23.2.1) of Abramovitz and Stegun.[35] Comparison of Eqs. (A3) and (A4) to Eq. (39) gives Eqs. (40) and (41) of the main text.

For $u=0$ one has Eq. (42):

$$g(k)=1-\psi(k,0)=2A\sum_{r>0}\frac{1-\cos(kr)}{r^{\mu+1-1/\nu}}\ . \tag{A5}$$

We again must have $\mu\nu>1$. For $\mu-1-1/\nu>1$, i.e., $\mu\nu>2\nu+1$ we may even expand the cosine up to the k^2 term and we expect $1-\psi(k,0)\sim C_2k^2$, as we subsequently show. Consider again first the case $\mu-1-1/\nu<1$, i.e., $1<\mu\nu<2\nu+1$. Reverting (A5) to integral form one has

$$g(k)\simeq 2A\int_\theta^\infty dr\frac{1-\cos(kr)}{r^{\mu+1-1/\nu}}\ . \tag{A6}$$

As before, we extend the integration to zero, a fact which introduces corrections of the order k^2. Setting now $y=kr$ one has

$$g(k)\simeq 2Ak^{\mu-1/\nu}\int_0^\infty dy\frac{1-\cos y}{y^\alpha}\ , \tag{A7}$$

with $\alpha=\mu+1-1/\nu$ and $1<\alpha<3$.

The integral in Eq. (A7) can now be readily evaluated by integration by parts. Depending on whether $1<\alpha<2$ or $2<\alpha<3$ holds, one integrates once or twice and makes use of the relations (3.761.4) or (3.761.9) in Gradshteyn and Ryzhik.[36] Both cases lead to

$$\int_0^\infty dy\frac{1-\cos y}{y^\alpha}=-\frac{\pi\sec(\alpha\pi/2)}{2\Gamma(\alpha)}\ , \tag{A8}$$

therefore

$$g(k)\simeq\frac{A\pi\,\mathrm{cosec}[\pi(\mu-1/\nu)/2]}{\Gamma(\mu+1-1/\nu)}k^{\mu-1/\nu}\ , \tag{A9}$$

a result also obtained by Gillis and Weiss[27] in their study of Eq. (A5). For $\mu\nu>2\nu+1$ the expansion of $\cos(kr)$ in (A5) to lowest order in k^2 gives

$$g(k)\simeq Ak^2\sum_{r>0}r^{-\mu+1+1/\nu}=A\zeta(\mu-1-1/\nu)k^2 \tag{A10}$$

where, again, we expressed the sum in terms of the ζ function. Comparing Eqs. (A9) and (A10) to Eq. (43) of the main text gives Eqs. (44) and (45).

In the discussion of the main text, for the integration leading to $P_0(u)$, Eq. (46), we approximated $1-\psi(k,u)$ through Eq. (37):

$$1-\psi(k,u)=C_1u^\gamma+C_2k^\epsilon\ , \tag{A11}$$

i.e., of a sum of two terms each having the structure of

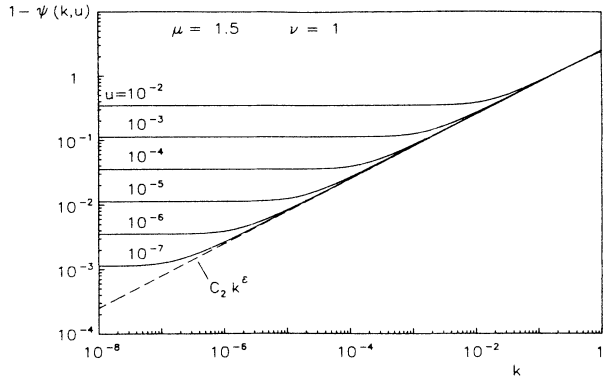

FIG. 6. The function $1-\psi(k,u)$ vs k is plotted on log-log scales. The parameters μ, ν are as indicated, u is given parametrically. The dashed line denotes the case $u=0$, $1-\psi(k,0)\sim C_2 k^{\epsilon}$, Eq. (43).

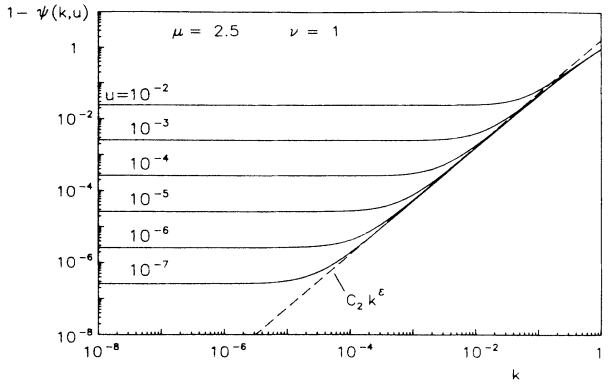

FIG. 7. Same as Fig. 6 but for the parameter $\mu=2.5$.

Eqs. (A3) or (A4) and Eqs. (A9) or (A10), respectively. In order to show that Eq. (A11) leads to a numerically correct behavior for $1-\psi(k,u)$ we display in Figs. 6 and 7 the situation for various parameters. Plotted are the numerically calculated $1-\psi(k,u)$ as a function of k on a log-log scale for various values of u. Also shown are the asymptotic $u=0$ forms, $1-\psi(k,0)\sim C_2 k^{\epsilon}$ which are given as broken lines. The exponents were chosen to be $\nu=1$ in both figures, while μ takes the values 1.5 and 2.5. In both figures the shapes of the functions $1-\psi(k,u)$ show a marked crossover from a u-dependent constant at $k \ll u$ to a $C_2 k^{\epsilon}$ behavior at $k \gg u$. This turns out to be the important fact in the integration in Eq. (46), as discussed in the main text.

Furthermore, in applications one should be well aware of the fact that Eq. (A11) is only a handy approximation. Thus it cannot be used in the calculation of $\langle r^2(t)\rangle$, which requires the exact determination of the second derivative of $\psi(k,u)$ with respect to k, see Eq. (17). For $\langle r^2(t)\rangle$ one has to proceed as exemplified in the main text.

To close this appendix we consider the integration in Eq. (46),

$$P_0(u)=\frac{C_1 u^{\gamma-1}}{\pi}\int_0^{\pi}\frac{dk}{C_1 u^{\gamma}+C_2 k^{\epsilon}}\ , \tag{A12}$$

where $0<\epsilon<2$, see Eq. (44). This form also appears in Ref. 37. For $\epsilon<1$ the integral converges even for $u=0$. The leading term of $P_0(u)$ is thus

$$P_0(u)\simeq\frac{C_1 u^{\gamma-1}}{C_2\pi}\int_0^{\pi}dk\ k^{-\epsilon}=\frac{C_1 u^{\gamma-1}}{C_2\pi^{\epsilon}(1-\epsilon)}\ . \tag{A13}$$

For $\epsilon>1$ the integral is dominated by the behavior of the integrand at small k. We thus can shift the upper integration limit to infinity. The change of variables $x=C_2 k^{\epsilon}/(C_1 u^{\gamma})$ leads to

$$P_0(u)=\frac{C_1^{1/\epsilon}u^{\gamma/\epsilon-1}}{C_2^{1/\epsilon}\epsilon}\mathrm{cosec}(\pi/\epsilon) \tag{A14}$$

where we used Eq. (3.222.2) of Gradshteyn and Ryzhik,[36]

$$\mathrm{cosec}(\pi/\epsilon)=\int_0^{\infty}dx\frac{x^{1/\epsilon-1}}{1+x}\ . \tag{A15}$$

Comparing Eqs. (A13) and (A14) to Eq. (47) gives Eq. (48) of the main text.

[1]A. S. Monin and A. M. Yaglom, *Statistical Fluid Mechanics* (MIT, Cambridge, MA, 1971), Vol. I; (1975), Vol. II.
[2]L. F. Richardson, Proc. R. Soc. London, Ser. A **110**, 709 (1926).
[3]G. K. Batchelor, Proc. Cambridge Philos. Soc. **48**, 345 (1952).
[4]G. K. Batchelor and A. A. Townsend, in *Surveys in Mechanics*, edited by G. K. Batchelor and R. M. Davies (Cambridge University Press, Cambridge, England, 1956), p. 352.
[5]A. Okubo, J. Oceanol. Soc. Jpn. **20**, 286 (1962).
[6]S. Grossmann, F. Wegner, and K. H. Hoffmann, J. Phys. (Paris) Lett. **46**, L575 (1985).
[7]M. F. Shlesinger and J. Klafter, Phys. Rev. Lett. **54**, 2551 (1985).
[8]J. Klafter, A. Blumen, and M. F. Shlesinger, Phys. Rev. A **35**, 3081 (1987).
[9]G. Zumofen, A. Blumen, J. Klafter, and M. F. Shlesinger, J. Stat. Phys. **54**, 1519 (1989).
[10]H. Scher and E. W. Montroll, Phys. Rev. B **12**, 2455 (1975).
[11]M. F. Shlesinger, J. Stat. Phys. **10**, 421 (1974).
[12]S. Alexander and R. Orbach, J. Phys. (Paris) Lett. **43**, L625 (1982).
[13]A. Blumen, J. Klafter, B. S. White, and G. Zumofen, Phys. Rev. Lett. **53**, 1301 (1984).
[14]A. Blumen, J. Klafter, and G. Zumofen, in *Optical Spectrosco-*

py of Glasses, edited by I. Zschokke (Reidel, Dordrecht, 1986), p. 199.
[15]E. W. Montroll and G. H. Weiss, J. Math. Phys. **6**, 167 (1965).
[16]A. Blumen and G. Zumofen, J. Chem. Phys. **77**, 5127 (1982).
[17]A. Blumen, J. Klafter, and G. Zumofen, in *Fractals in Physics,* edited by L. Pietronero and E. Tosatti (North-Holland, Amsterdam, 1986), p. 399.
[18]J. Klafter and R. Silbey, Phys. Rev. Lett. **44**, 55 (1980).
[19]M. F. Shlesinger and J. Klafter, in *On Growth and Form,* edited by H. E. Stanley and N. Ostrowski (Nijhoff, Amsterdam, 1985), p. 279.
[20]M. F. Shlesinger, J. Klafter, and Y. M. Wong, J. Stat. Phys. **27**, 499 (1982).
[21]H. Takayasu, Prog. Theor. Phys. **72**, 471 (1984).
[22]M. F. Shlesinger, B. J. West, and J. Klafter, Phys. Rev. Lett. **58**, 1100 (1987).
[23]G. H. Weiss and R. J. Rubin, Adv. Chem. Phys. **52**, 363 (1983).
[24]J. W. Haus and K. W. Kehr, Phys. Rep. **150**, 263 (1987).
[25]J. W. Haus and K. W. Kehr, Phys. Rev. B **36**, 5639 (1987).
[26]B. B. Mandelbrot, *The Fractal Geometry of Nature* (Freeman, San Francisco, 1982).
[27]J. Gillis and G. H. Weiss, J. Math. Phys. **11**, 1308 (1970).
[28]A. Blumen, G. Zumofen, and J. Klafter, J. Lumin. **40/41**, 641 (1988).
[29]P. Argyrakis and R. Kopelman, Phys. Rev. B **22**, 1830 (1980).
[30]K. Kehr and P. Argyrakis, J. Chem. Phys. **84**, 5816 (1986).
[31]G. Zumofen, A. Blumen, and J. Klafter, J. Chem. Phys. **82**, 3198 (1985); **84**, 6679 (1986).
[32]P. Dimotakis, R. C. Lye, and D. Z. Papantoniou, 15th International Symposium on Fluid Dynamics, Jachranka, Poland, 1981 (unpublished).
[33]K. R. Sreenivasan and C. Meneveau, J. Fluid. Mech. **173**, 357 (1986).
[34]E. T. Whittaker and G. N. Watson, *Modern Analysis* (Cambridge University Press, Cambridge, England, 1927), Sec. 12.21, p. 244.
[35]*Handbook of Mathematical Functions,* edited by M. Abramovitz and I. A. Stegun (Dover, New York, 1972).
[36]*Table of Integrals, Series and Products,* edited by I. S. Gradshteyn and I. M. Ryzhik (Academic, New York, 1980).
[37]H. Weissmann, G. H. Weiss, and S. Havlin (unpublished).